# Pd diffusion on MgO(100): The role of defects and small cluster mobility

Lijun Xu [a], Graeme Henkelman [b,*], Charles T. Campbell [a], Hannes Jónsson [a,c]

[a] *Department of Chemistry 351700, University of Washington, Seattle, WA 98195-1700, United States*
[b] *Department of Chemistry and Biochemistry, University of Texas at Austin, 1 University Station Stop A5300, Austin, TX 78712-0165, United States*
[c] *Faculty of Science, VR-II, University of Iceland, 107 Reykjavík, Iceland*

## Abstract

Density functional theory is used to explore the energy landscape of Pd atoms adsorbed on the terrace of MgO(100) and at oxygen vacancy sites. Saddle point finding methods reveal that small Pd clusters diffuse on the terrace in interesting ways. The monomer and dimer diffuse via single atom hops between oxygen sites with barriers of 0.34 eV and 0.43 eV respectively. The trimer and tetramer, however, form 3D clusters by overcoming a 2D–3D transition barrier of less than 60 meV. The trimer diffuses along the surface either by a walking or flipping motion, with comparable barriers of ca. 0.5 eV. The tetramer rolls along the terrace with a lower barrier of 0.42 eV. Soft rotational modes at the saddle point lead to an anomalously high prefactor of $1.3 \times 10^{14} \, s^{-1}$ for tetramer diffusion. This prefactor is two order of magnitude higher than for monomer diffusion, making the tetramer the fastest diffusing species on the terrace at all temperatures for which diffusion is active (above 200 K). Neutral oxygen vacancy sites are found to bind Pd monomers with a 2.63 eV stronger binding energy than the terrace. A second Pd atom, however, binds to this trapped monomer with a smaller energy of 0.56 eV, so that dimers at defects dissociate on a time scale of milliseconds at room temperature. Larger clusters bind more strongly at defects. Trimers and tetramers dissociate from monomer-bound-defects at elevated temperatures of ca. 600 K. These species are also mobile on the terrace, suggesting they are important for the ripening observed at ⩾600 K during Pd vapor deposition on MgO(100) by Haas et al. [G. Haas, A. Menck, H. Brune, J.V. Barth, J.A. Venables, K. Kern, Phys. Rev. B 61 (2000) 11105].
© 2006 Elsevier B.V. All rights reserved.

*Keywords:* Density functional calculation; Models of surface kinetics; Palladium; Magnesium oxide

## 1. Introduction

The growth, migration and agglomeration of small metal clusters on oxide surfaces are of importance in many technological applications, including catalysis and chemical sensing by oxide-supported metal nanoparticles, the production of metal thin films and coatings, and the fabrication of microelectronic, magnetic, photonic and photovoltaic devices [1–7]. The dynamics of small metal clusters on oxides is also of importance in fundamental

scientific research concerning such systems. Key issues include the mechanisms and kinetics of diffusion of the metal adatoms and metal clusters, their nucleation dynamics and sintering mechanisms, the role of surface defects in these processes, and how the size and distribution of the metal clusters influence their energetics, thermal stability, electronic properties and functionality in applications.

A widely held view of the growth of late transition metal films on single crystal oxide surfaces by vapor deposition is that metal atoms land primarily on flat terraces and diffuse over the surface by hopping from one site to another. Step edges or point defects, however, bind the metal adatoms so strongly that they get trapped there. A second diffusing adatom which encounters such a metal-defect complex will

---

* Corresponding author. Tel.: +1 512 471 4179; fax: +1 512 232 4655.
  *E-mail address:* henkelman@mail.utexas.edu (G. Henkelman).

also get trapped there, and by the further addition of other diffusing adatoms, the metal cluster builds up at the defect site [3,4,8]. This is referred to as heterogeneous nucleation. In homogeneous nucleation, the clusters nucleate instead on the majority (terrace) sites. However, the details of the elementary steps and intermediate structures involved are still poorly understood, and indeed it is not even clear whether this is the proper mechanism. Certainly, no atomistic model that reproduces the growth kinetics for any metal-on-oxide system has ever been developed which is based on independently determined kinetic parameters.

Since oxide-supported metal clusters with diameters less than 4 nm are very unstable relative to large metal particles, they also tend to sinter into fewer, larger clusters, especially at high temperatures [9]. This is a major mechanism for deactivation of oxide-supported transition metal catalysts. Sintering can occur either by "Ostwald ripening", in which individual metal atoms (possibly in the form of a complex with another species, hence "monomers") leave a metal cluster, diffuse over the support, and join another metal cluster, or by "cluster diffusion/agglomeration" wherein the metal clusters diffuse across the oxide surface, encounter other clusters and merge into one (as do two water droplets when they touch) [4,9–16]. Again, the details of the elementary steps and intermediate structures involved are still poorly understood, and no atomistic model that fully reproduces sintering kinetics has been developed yet. Nevertheless, a complete understanding of sintering kinetics would be very valuable in the development of new catalysts.

In this paper, we combine density functional theory (DFT) with the nudged elastic band method (NEB) [17,18], the dimer method [19,20], and harmonic transition state theory [21,22] to estimate the structures, energies, entropies, diffusion mechanisms, transition states and diffusion kinetic parameters of small metal clusters for a prototypical metal-on-oxide system. The results reveal several important phenomena involving clusters larger than dimers which have previously been ignored but which clearly need to be considered when analyzing the growth and sintering of metal islands on oxide surfaces and the role of point defects. The energies of the many cluster structures reported here also will help any effort to develop a simple parameterized Pd–MgO(100) potential for molecular dynamics simulations of growth and sintering kinetics.

To date, the most thoroughly studied metal/oxide system in terms of structural elucidation during growth and sintering is Pd on MgO(100) [3,23–29]. We have, therefore, chosen to carry out theoretical calculations on this system, but its properties are qualitatively typical of many other interesting metal/oxide systems [4]. Experimental measurements of Pd islands grown by metal atom deposition on MgO(100) at low temperature have shown that the number density of the islands is remarkably insensitive to the surface temperature during growth [30]. This is a clear indication that defects play an important role in the growth process. It is well known that oxide surfaces tend to have

a high density of point defects (typical estimates being $10^{12}$–$10^{13}$ cm$^{-2}$ [31]) in addition to steps and grain boundaries. HREELS spectra have been assigned and interpreted in terms of neutral oxygen vacancies, so called F-centers, where an oxygen atom has been removed from the surface [32]. It has also been suggested that di-vacancies are present where both a Mg- and O-atom are missing [31] and, in some cases, charged oxygen vacancies [32,33]. We have assumed that the defects nucleating Pd clusters are neutral oxygen vacancies. This is consistent with experiments using CO as a chemical marker to determine the Pd bonding at surfaces. The vibrational frequency of CO bound to Pd atoms at point defects on MgO are observed to be red-shifted relative to Pd–CO [34]. Theoretical calculations, however, show a blueshift for Pd atoms at charged F-centers [35], suggesting that the primary point defects are (neutral) F-centers.

Measurements of Pd island densities from vapor deposition experiments on MgO(100) have been previously analyzed by applying the common growth model mentioned above. Various energy parameters, such as monomer diffusion activation energy, Pd/defect trapping energy, and dimer binding energy, were adjusted to fit the measured island density over a wide range of substrate temperatures. There are two problems, however, with this simple picture of Pd island formation. Different types of experiments lead to different sets of best-fit parameters [3,30], and the derived energy landscape is inconsistent with first principles calculations. Specifically, a strong dimer binding energy of 1.2 eV is required to match the ripening observed at 600 K [30]. Giordano et al. find the binding energy of a second Pd atom to an adatom/F-center complex to be very weak (0.39 eV), insignificantly larger than the dimer binding energy on the defect-free terrace (0.35 eV) [36]. The weak binding has also been seen for Pt on MgO(100), in which a Pt adatom prefers the terrace over binding to another adatom trapped at an F-center [37]. This suggests that some assumptions in the model must be inaccurate.

We present here theoretical results that indicate a different role for F-centers in the Pd-island growth process, which presumably will also be important in understanding sintering kinetics. A brief communication of some of these kinetic results has been published previously [38] (see also Ref. [39]). Here we describe a systematic atomic-scale study of the formation and diffusion mechanisms of small Pd clusters (Pd$_1$ to Pd$_4$) on MgO(100), with and without oxygen vacancy defects.

## 2. Calculation methodology

Calculations are performed with the Vienna Ab initio Simulation Package, VASP, using the PW91 functional [40] and ultra-soft pseudo-potentials of the Vanderbilt form [41]. A plane wave cutoff of 270 eV, appropriate for the pseudo-potentials, and a $\Gamma$ point sampling of the Brillouin zone, are found to be sufficiently converged, as shown

in Appendix A. Spin polarization was tested for each cluster size. The only cluster found to have a magnetic moment is the tetramer, for which spin polarization reduces the adsorption energy by 0.12 eV. For this reason, all calculations of the tetramer are done with spin polarization.

The MgO(100) surface is modeled as a slab with three layers, using either 24 or 36 atoms per layer in each unit cell. The simulation box is chosen with a height of 16.7 Å, perpendicular to the (100) surface. The lower two layers are held frozen at the optimal DFT lattice constant of 4.23 Å, which compares well with the 4.21 Å experimental lattice constant. Atomic positions in the top layer are fully optimized in each calculation. When Pd is adsorbed on the surface, the substrate atoms are found to relax by no more than 0.1 Å, and adsorption energies are lowered by 0.1–0.2 eV. The relative energies of different cluster sizes and geometries, however, are largely unaffected by the relaxation of the top layer. Furthermore, the addition of more MgO layers and the relaxation of more surface layers do not change our results (see Appendix A).

Adsorption energies, $E_{ads}$, for a cluster of $n$ Pd atoms on the MgO surface are calculated as

$$-E_{ads} = E_{sys} - nE_{Pd} - E_{MgO} \qquad (1)$$

where $E_{sys}$ is the energy of $n$ Pd atoms adsorbed on the MgO surface, $E_{Pd}$ is the energy of an isolated gas phase Pd atom, and $E_{MgO}$ is the energy of the MgO substrate.

Diffusion barriers are calculated by finding saddle points on the potential surface. When both the initial and final state is known for a diffusion process, the nudged elastic band (NEB) method [17,18] is used to determine the reaction mechanism and diffusion barrier. The dimer saddle point finding method [19,20] was also used both to investigate the possibility of unexpected mechanisms leading from known minima, and to efficiently converge upon nearby saddle points. All geometries are optimized so that the maximum force in every degree of freedom is less than 0.001 eV/Å. Normal mode frequencies are calculated with a finite difference method for all relaxed atoms at stationary points to evaluate the entropy in the harmonic approximation, and the prefactor of reaction rates. Tests show that finite difference displacements ranging from 0.005 to 0.001 Å resulted in prefactors differing by less than 10% from converged values. Reaction rates are estimated using the harmonic form of transition state theory [21,22],

$$k_{hTST} = \frac{\prod_{i=1}^{3N} \nu_i^{init}}{\prod_{i=1}^{3N-1} \nu_i^{\ddagger}} e^{-(E^{\ddagger} - E^{init})/k_B T}. \qquad (2)$$

In this expression $E^{\ddagger}$ is the energy of the saddle point, $E^{init}$ is the energy of the local minimum corresponding to the initial state, $k_B$ is Boltzman's constant, $T$ is the temperature, $N$ is the number of moving atoms, and $\nu_i$ are the real normal mode frequencies at the saddle point ($\ddagger$) and initial state (init) respectively.

## 3. Results

### 3.1. Monomer

Three binding sites were considered for the adsorption of Pd atoms. The Mg and O sites, directly above Mg and O ions respectively, and the hollow site between two Mg and two O ions. We find that the Pd monomer only binds at the O-site, in agreement with previous studies [42,43]. The monomer adsorption energy is found to be 1.37 eV with a Pd–O distance of 2.09 Å. The oxygen on which the Pd sits relaxes inward by 0.05 Å relative to the topmost plane surface ions. The monomer binding energy is relatively insensitive to the details of the DFT calculation. Cluster and supercell models using the BP and PW91 density functionals give a binding energy of ca. 1.4 eV [44–46,36].

A Bader atoms-in-molecules (AIM) analysis of the charge density [47,48] shows a small but noticeable and well localized charge transfer of 0.15 e from the substrate oxygen ion to the on-top adsorbed Pd adatom and almost no charge transfer from Mg atoms in the substrate. The direction and amount of charge transferred between O and Pd is close to the value of 0.19 e given by a recent AIM calculation from a very different kind of DFT calculation, using a cluster model with the B3LYP functional [49]. An earlier cluster model calculation using the BLYP functional with and without a relativistic correction predicted a charge transfer from O to Pd of 0.2 and 0.3 e respectively using a Mulliken population analysis [50]. The agreement between these different calculations suggests that the charge transfer from O to Pd is a robust prediction of DFT calculations.

The diffusion mechanism for a Pd monomer (see Fig. 1) is found to be a direct hopping process between oxygen sites. In the saddle geometry, the Pd atom sits above a hollow site. The energy barrier for monomer diffusion is 0.34 eV; consistent with what has been found previously [36]. An Arrhenius prefactor for monomer hopping is
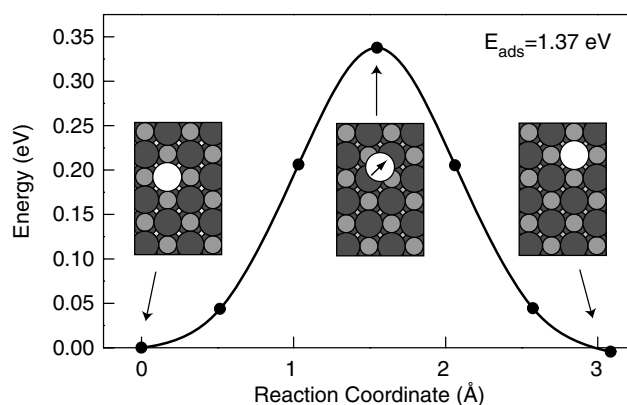


Fig. 1. Pd monomer binds to O-sites with adsorption energy 1.37 eV, and diffuses via a hop mechanism. White circles represent Pd atoms, small gray circles Mg atoms and large dark gray circles are O atoms.

calculated from the harmonic approximation (Eq. (2)) as $7.4 \times 10^{11}$ s$^{-1}$. This is approximately an order of magnitude less than a typical prefactor of $5 \times 10^{12}$ s$^{-1}$.

The monomer is found to bind very strongly to a neutral oxygen vacancy (F-center) with an adsorption energy of 4.0 eV, in agreement with a recent study [36] using both cluster and supercell models.

### 3.2. Dimer

The most stable dimer on the MgO(1 0 0) terrace, (labeled as D1, as shown in Fig. 2), has two Pd adatoms sitting at neighboring oxygen sites. The Pd–Pd distance of 2.81 Å is smaller than the distance of 3.00 Å between oxygen atoms in the surface. The Pd dimer sits 2.12 Å above the MgO substrate surface plane and has an adsorption energy of 3.28 eV, relative to two isolated atoms in the gas phase. A Bader analysis shows a charge transfer, similar to the monomer, of 0.15 e to each Pd adatom from the oxygen atom beneath. The dimer binding energy, defined as the energy released when two Pd monomers on the MgO(1 0 0) terrace form a dimer, is found to be 0.54 eV.

The second most stable dimer, labeled as D2, has two Pd adatoms adsorbed on next nearest neighboring oxygen sites, with a Pd–Pd distance of 3.03 Å and a Pd-surface plane distance of 2.10 Å. The total adsorption energy for D2 is 2.96 eV, which is 0.22 eV larger than the adsorption energy of the monomer.

The next most stable configurations, D3 and D4 (see Fig. 2), both have adsorption energies of 2.73 eV, within 0.01 eV of that for two separate monomers. The Pd–Pd interactions are weak enough that they can be considered as two non-interacting monomers. This is consistent with the fact that the monomer adsorption energy can be found accurately with a periodic substrate containing only four Mg and four O atoms per layer in each unit cell [42,43].

Finally, we considered a vertical dimer in which the two Pd atoms are arranged perpendicular to the surface above an oxygen site. Although this geometry is found to be a (shallow) local minimum, it is almost an eV less stable than D1, and is not relevant to ripening dynamics.

The dimer binds at an oxygen vacancy with an adsorption energy of 5.94 eV and a geometry similar to D1 with a missing oxygen ion beneath one of the Pd atoms. The dimer binding energy at the defect, relative to two monomers, one on an F-center, is 0.57 eV. This is somewhat higher than the 0.37 eV binding energy found using the B3LYP functional (which is expected to be more accurate than the PW91 functional used in this study) [36].

### 3.3. Dimer diffusion

To determine the mechanisms of dimer diffusion, we did a systematic study of saddle points between the Pd dimer configurations described above. The most relevant three such transitions are shown in Fig. 3. The lowest barrier of 0.43 eV corresponds to the partial dissociation of D1 to D2 (D1-2), by a single Pd hopping mechanism. This process has a prefactor of $2.5 \times 10^{11}$ s$^{-1}$. The reverse barrier is 0.1 eV and has a prefactor that is 60 times larger. Fig. 4 shows how two such processes lead to net diffusion through a partially dissociated intermediate structure.

D1 can also diffuse by a concerted slide mechanism (D1-1) along the dimer axis with a barrier of 0.60 eV, and it can dissociate to D3 (two isolated monomers) with a barrier (D1-3) of 0.84 eV.

### 3.4. Trimer

Trimer configurations are constructed by adding one Pd atom to the D1 and D2 dimer configurations. The lowest energy trimer, labeled as T1 in Fig. 5, is constructed by adding a Pd atom on the bridge between the atoms in D1. Remarkably, this vertical quasi-equilateral triangle structure with the Pd–Pd distances of 2.52 Å has the largest adsorption energy of 5.69 eV (1.89 eV/atom) relative to 3 Pd atoms in gas phase [51]. The second most stable trimer, T2, with an adsorption energy of 5.42 eV (1.81 eV/atom) can be constructed in a similar manner as T1, using D2 as the base. The Pd bonds in T2 are stretched to 2.64 Å between the base atoms, and 2.50 Å between the top atom and the base atoms. T2 is less stable than T1 in the same way that D2 is less stable than D1. The binding
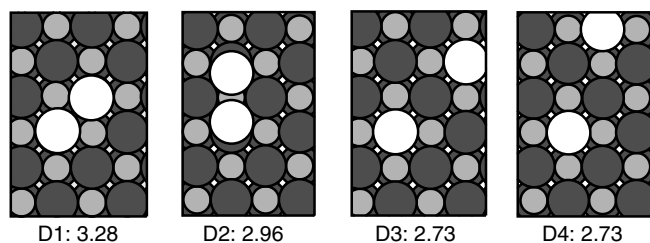


Fig. 2. The four most stable dimer configurations, and adsorption energies in eV. The adsorption energy of D3 and D4 is the same, indicating that the monomers in both configurations are separated beyond their interaction distance.
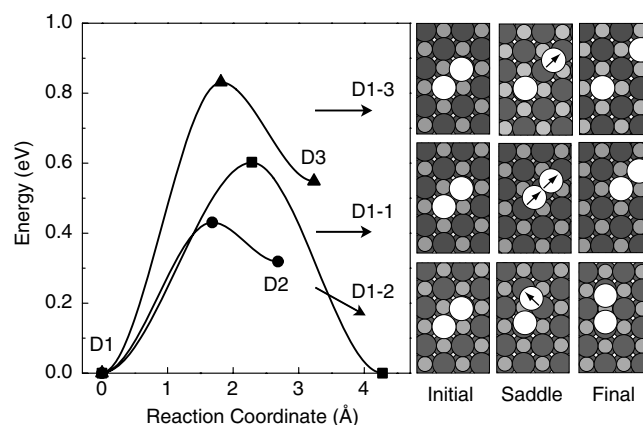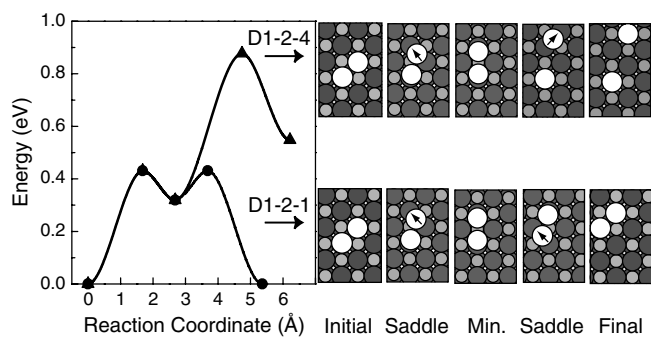


Fig. 3. Pd dimer diffusion pathways.

Fig. 4. Dissociation and complete diffusion mechanism of the Pd dimer.
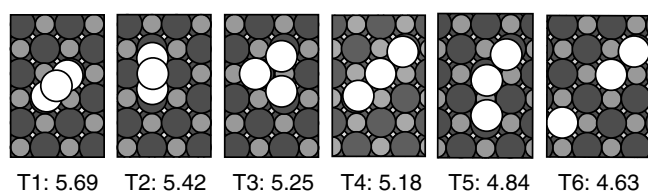


Fig. 5. Most stable Pd trimer configurations: $E_{ads}$ (eV).

energy of T1 (relative to D1 plus a monomer) on the flat MgO(1 0 0) terrace is 1.06 eV.

Trimer configurations lying flat on the MgO(1 0 0) surface are constructed by placing a Pd atom next to the D1 and D2 dimers. The most stable flat timer, T3, has a Pd atom next to D1 forming a triangle on oxygen sites with two Pd–Pd bond lengths of 2.72 Å and one stretched bond of 3.02 Å. T3 has an adsorption energy of 5.25 eV (1.75 eV/ atom), which is 0.44 eV less stable than the lowest energy vertical trimer, T1; similarly, vertical Pd trimers have been also predicted to be 0.4 eV more stable than flat ones in a recent study of Pd$_3$/$\alpha$-Al$_2$O$_3$(0 0 0 1) [52].

The fourth trimer configuration, T4, is simply a linear structure, which can be constructed by adding a Pd atom to the end of the D1 dimer configuration. The Pd–Pd bond lengths are 2.74 Å and the energy is 5.18 eV (1.73 eV/ atom). This T4 trimer can partially dissociate to the bent trimer (T5) or fully dissociate to a monomer plus a dimer (i.e., structure T6) in a similar mechanism to the D1-2 and D1-3 processes shown in Fig. 3.

A Bader analysis of T1 shows that 0.1 e charge transfers from the MgO substrate to each of the two Pd atoms in contact with the substrate, while the extra charge on the top Pd atom is smaller (0.06 e).

Adsorption of trimers on F-centers has been studied by Giordano et al. with a very similar model. The two most favorable trimer configurations were found to be almost degenerate in energy. One structure is a tilted vertical tri- mer similar to T3 with one of two oxygen atoms being re- moved to form the F-center, and the other is a bent linear trimer similar to T4 with the oxygen atom beneath the cen- tral Pd atom missing to form the F-center [51]. Our calcu- lations confirm this result and predict an adsorption energy

of 8.08 eV. The trimer binding energy (i.e., the energy of the T1/F-center complex minus that of the D1/F-center complex plus the monomer on a terrace) is found to be 0.76 eV; very similar to the value of 0.75 eV found previ- ously [51].

### 3.5. Trimer diffusion

The lowest energy migration pathways for the Pd trimer are shown in Fig. 6. The most stable trimer (T1) diffuses via a walking mechanism similar to the D1-2 dimer diffusion shown in Fig. 3. The topmost Pd atom remains above
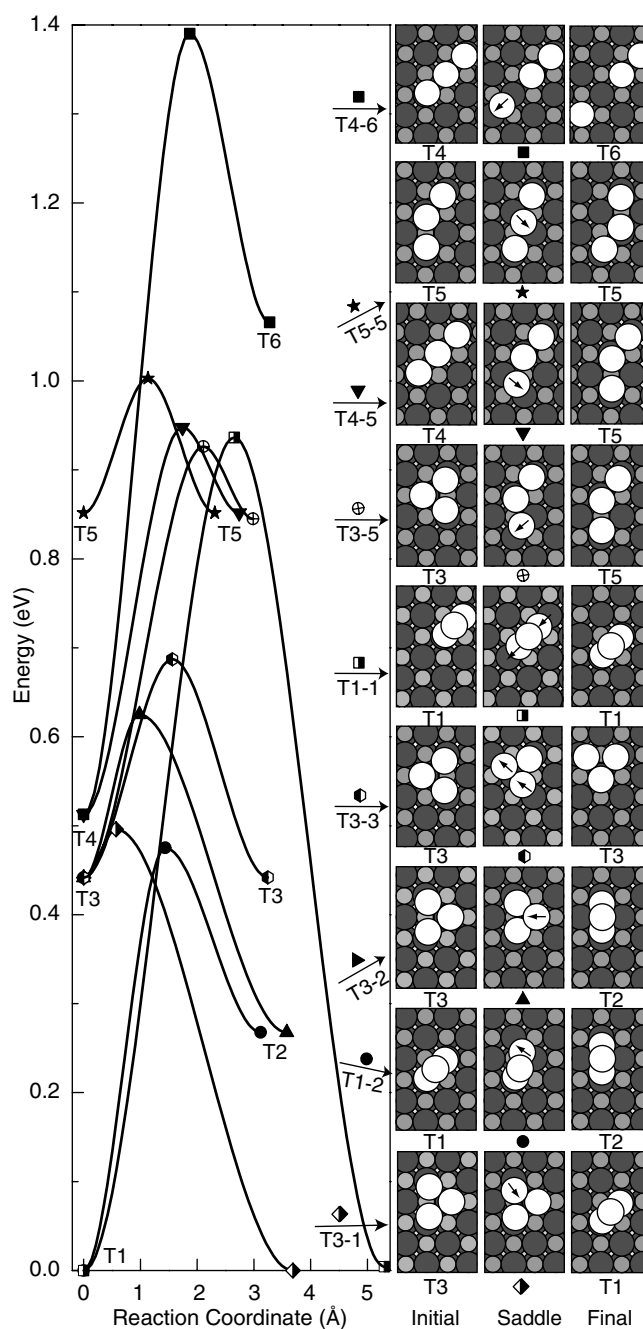


Fig. 6. Pd trimer diffusion pathways.

and between the base dimer during its lowest energy migration process (T1-2). The barrier for this step is 0.48 eV, which is similar to that found for dimer diffusion (0.43 eV); the barrier for the reverse process (T2-1) is only 0.21 eV. Fig. 7 (lower pathway) shows how the walking mechanism can lead to net diffusion of the trimer.

A second, flipping mechanism, has a very similar barrier to the walking mechanism: T1 can diffuse via the flat configuration T3 (see Fig. 6). By crossing a slightly higher barrier of 0.50 eV, the top atom from T1 can flip down to the surface, forming T3, from which a different atom can lift onto the other two forming T1 in a different location (see Fig. 7, process T1-3-1). The reverse step has a small barrier of only 0.055 eV, so that the overall barrier for diffusion by this flipping mechanism is only 0.50 eV. In a similar way, T3 can diffuse via the T2 vertical configuration (process T3-2), crossing the barrier of 0.18 eV or the overall barrier of 0.63 eV with respect to the lowest energy T1 structure.

The T1-3 (flipping) and T1-2 (walking) mechanisms have similar barriers (0.50 eV and 0.48 eV respectively). A higher prefactor of $1.1 \times 10^{13}$ s$^{-1}$ for the flipping mechanism as compared to $5.4 \times 10^{10}$ s$^{-1}$ for the walking mechanism, means that the flipping mechanism will dominate trimer diffusion at high temperature; in fact, it is even slightly favored at liquid nitrogen temperature (77 K).

The flat T3 trimer can change configuration via a double-slide mechanism in which two Pd atoms slide across hollow sites along the short edge of the flat triangle (process T3-3). The barrier for this mechanism is 0.25 eV with respect to the flat trimer T3, and 0.69 eV with respect to the lowest energy trimer T1. Not only is the overall barrier very high compared to T1-2 and T1-3 but also this mechanism alone does not lead to trimer diffusion: the trimer remains trapped in a square of five oxygen binding sites.

Finally, the higher energy flat trimer structures (T4, T5 and T6 in Fig. 5) can diffuse on the MgO(100) surface without forming the low-energy vertical structure T1 and T2. These processes (including T3-5, T4-5, T5-5 and T4-6

shown in Fig. 6) involve single Pd atom hops between oxygen sites with barriers in the range 1.0–1.4 eV with respect to T1. At temperatures less than 1000 K these high energy processes will not play significant roles due to the overwhelming stability of the vertical structures.

## 3.6. Tetramer

Similar to the Pd trimer, both 2D (flat) and 3D (tetrahedral) structures are stable. Two tetramer configurations were studied on a larger MgO unit cell, with 36 atoms per layer. The tetramer is stable in a flat square planar configuration [53,54], in which each Pd atom is bound to an oxygen site. This structure has an adsorption energy of 7.71 eV (1.93 eV/atom), with Pd–Pd bond distances of 2.55 Å and Pd–O distances of 2.28 Å. As with the flat trimer, the flat tetramer can easily convert to a more stable 3D structure. Fig. 8 shows the minimum energy path, in which a Pd atom in the 2D square planar structure rises on top of the other three atoms to form a 3D tetrahedron, while crossing a barrier of only 0.04 eV.

The 3D tetrahedral structure, with an adsorption energy of 8.80 eV (2.20 eV/atom) is more stable than the 2D planar structure because it has more Pd–Pd bonds, each of which is stronger than the Pd–O bonds to the surface. The Pd–O bond length is 2.23 Å, and the Pd–Pd bond length is 2.59 Å. The base triangle of Pd atoms is close to equilateral (angles of 56.5°, 56.5° and 67.0°) despite the rectangular MgO(100) surface. This structure has been confirmed as the most stable tetramer configuration previously [51]. The binding energy of the tetrahedron tetramer is 1.7 eV, i.e., lower by 1.7 eV than the energy of T1 and a monomer.

A Bader analysis of the tetrahedron tetramer on MgO(100) shows some combined features of the flat and vertical trimers. The two equivalent Pd atoms on the base each have 0.17 e extra charge, while the third has a smaller charge of 0.05 e. The top Pd atom also shows a small extra charge of 0.09 e.

Removing an oxygen atom from below one of the Pd atoms in the tetrahedron base leads to a tetrahedron/F-
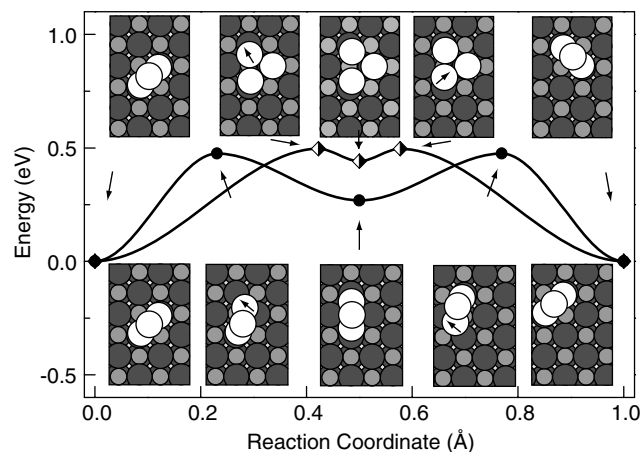


Fig. 7. Diffusion mechanism of the vertical trimer (T1). Upper insets show the flipping mechanism (T1 → T3 → T1) and lower insets show the walking mechanism (T1 → T2 → T1).
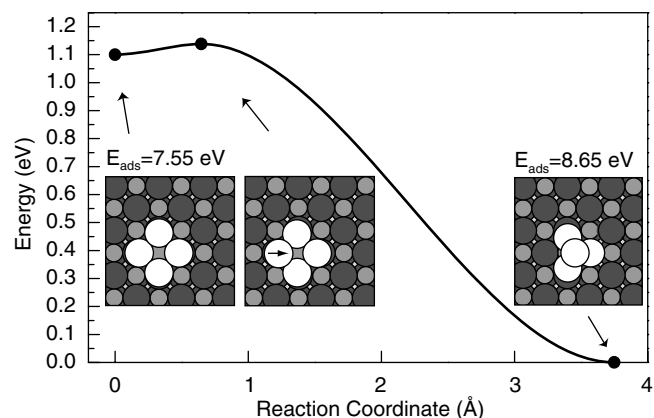


Fig. 8. Low energy barrier for the 2D–3D tetramer transition.

center complex. The binding energy of the tetramer, as compared to the T1/F-center complex plus a monomer on the flat terrace is 1.4 eV.

## 3.7. Tetramer diffusion

Due to the greater stability of the tetrahedron on the MgO(100), and the low 2D–3D transition barrier, the tetrahedron configuration will dominate tetramer dynamics on the MgO(100) surface. The lowest energy tetrahedron diffusion paths are shown in Fig. 9.

A qualitatively new type of mechanism for cluster diffusion was found with this tetramer, in which the tetramer rolls to a new binding site on the surface. We call this the "rollover" mechanism. There are two such processes, labeled as roll-I and roll-II in Fig. 9, in which a base atom and the top atom roll over (i.e., rotate around) the axis formed by the other two base atoms. The higher energy process, roll-II does not lead to net diffusion, but the lower energy, roll-I process, with a barrier of only 0.42 eV, does. This rollover mechanism was found to be the lowest barrier pathway for tetramer diffusion. Once the tetrahedral tetramer is formed, it will rapidly diffuse as a unit by this mechanism at room temperature, as shown in Fig. 10. The 1.14 eV barrier (labeled as 2D–3D in Fig. 9) required to form the flat tetramer from this tetrahedron is highly unfavorable.

Two processes were found which do not, by themselves, lead to tetramer diffusion, but do allow diffusion when combined sequentially. The first "rotation" process (rot-I) with a low barrier of 0.15 eV involves the hop of a single base Pd atom, and the second (rot-II) with a barrier of 0.51 eV involves the concerted slide of two base Pd atoms.
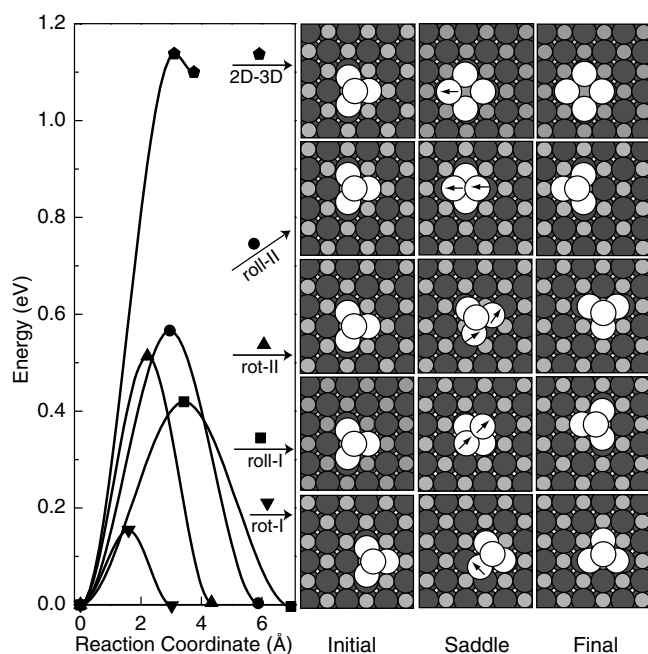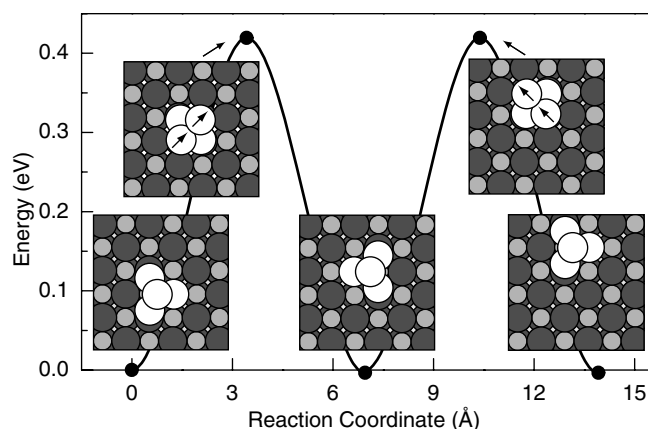


Fig. 10. The Pd tetrahedron rolls over the MgO(100) surface with a low barrier of 0.42 eV.
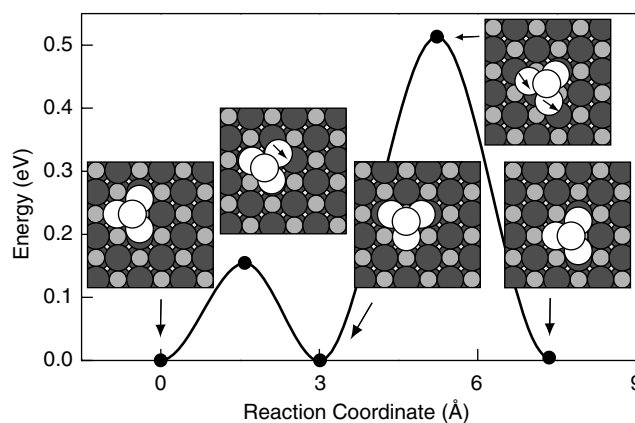


Fig. 11. Pd tetramer diffusion via two rotation mechanisms.

This second mechanism is analogous to the T3-3 trimer process, shown in Fig. 6. There is no trimer mechanism corresponding to the first (rot-I) mechanism; the diffusing atom moves on top of the other into the intermediate minimum T1. In both cases, the tetrahedron remains trapped in a square of oxygen binding sites. The combination of the two mechanisms leads to net diffusion, with an overall barrier of 0.51 eV (see Fig. 11).

Prefactor calculations show that the roll-I mechanism has a very large prefactor: $1.3 \times 10^{14}\ s^{-1}$ and the roll-II mechanism has a prefactor of $1.1 \times 10^{13}\ s^{-1}$, while the rot-I and rot-II mechanisms have prefactors of $2.3 \times 10^{13}\ s^{-1}$ and $1.0 \times 10^{13}\ s^{-1}$ respectively. Hence, the rollover (roll-I) mechanism is favored both by energy and entropy.

## 3.8. Binding at oxygen vacancies

The binding energies of small Pd clusters to a neutral oxygen vacancy are tabulated in Table 1. Here, the binding energy for a cluster ($Pd_n$) at an F-center is defined as the energy released when a smaller cluster ($Pd_{n-1}$) from the terrace combines with a Pd monomer trapped at the F-center. The calculations show that adsorbed monomers are



Fig. 9. Pd tetramer diffusion pathways.

Table 1
The binding energy ($E_b$) of a $Pd_n$ ($n = 2$–5) cluster at an F-center (neutral oxygen vacancy site)

| Pd cluster on F-center | $E_{ads}(Pd_n, F)$ (eV) | $E_{ads}(Pd_n)$ (eV) | $E_b(Pd_n, F)$ (eV) |
|---|---|---|---|
| Monomer | 4.01 | 1.37 | – |
| Dimer | 5.94 | 3.28 | 0.56 |
| Trimer | 8.08 | 5.72 | 0.79 |
| Tetramer | 10.85 | 8.79 | 1.12 |
| Pentamer | 13.63 | 11.55 | 0.83 |

$E_b$ is calculated as $E_b(Pd_n, F) = E_{ads}(Pd_n, F) - E_{ads}(Pd_1, F) - E_{ads}(Pd_{n-1})$, where $E_{ads}(Pd_n, F)$ is the adsorption energy of the $Pd_n$ cluster on an F-center relative to the gas-phase Pd atoms and the relaxed MgO(100) with an F-center while $E_{ads}(Pd_{n-1})$ refers to the adsorption energy on the terrace. The most stable structures for $Pd_n$ ($n = 1$–4) clusters bound to F-centers were assumed to be those found by Giordano et al. [51].

strongly trapped at F-centers (by 2.63 eV). A second monomer, however, binds less strongly (0.56 eV). Larger adsorbed clusters ($n = 2$–4) bind somewhat more strongly to the monomer/F-center complex, with energies in the range 0.8–1.1 eV.

# 4. Discussion

## 4.1. Structure of Pd clusters

DFT calculations have been used to understand the bonding between Pd clusters and the MgO(100) surface. Our calculations are consistent with previous theoretical predictions that oxygen sites are favorable for monomer adsorption [55,50,56,46,43]. Recent in situ Grazing Incident X-ray Scattering (GIXS) studies also confirmed that Pd adatoms adsorb at oxygen anions [25,26], in contrast to an earlier surface (extended) electron energy loss fine structure (SEELFS) study which suggested that the Pd adatoms bind to magnesium sites [57]. The Pd-surface distance for monomers is calculated here to be 2.09 Å, consistent with previous calculations [43–46]. Experimental measurements of $2.22 \pm 0.03$ Å for 1 ML Pd deposited on MgO(100) [25,26] are somewhat larger, perhaps due to the weaker Pd–O bonds expected in a Pd monolayer. Support for this can be seen in calculations of the flat tetramer and a Pd monolayer, which show a Pd–O bond length of ca. 2.28 Å, showing that the Pd–O bond length does increase with Pd island size.

The competition between Pd–O and Pd–Pd bonding is also shown in the evolution of cluster shape from dimers to tetramers: Pd clusters tend to assume vertical or three-dimensional structures. Only the dimer is most stable as a flat (i.e., 2D) island. Experimental measurements have found three-dimensional truncated octahedral shape for larger Pd particles on MgO(100) [3,29].

As many properties of materials and chemical processes can be explained directly and indirectly by the (re-)distribution of electron density within the material or upon to the change, it is reasonable to look into the charge density involved in the adsorption energetics. Our Bader charge analysis shows a clear charge transfer between MgO and Pd adatoms as electron density transfer from oxygen to palladium. This is different than most experimental measurements for similar metals on semiconducting oxides such as $TiO_2$ and ZnO, where the direction of charge transfer can be assessed [4]. (Such measurements are not possible on insulators like MgO). This calculated charge transfer direction is also verified in Mulliken charge analysis of DFT results for the same system [50]. Repulsion between the negative charges on the Pd atoms in flat-lying clusters may contribute to the driving force for trimers to stand vertically on the surface and larger clusters to be 3D.

Our charge analysis also shows that charge transfer is localized to the Pd–O bond. Pd atoms separated from the MgO surface, such as the topmost atom in 3D clusters, are charged by less than 0.1 e. This leads to a possible explanation as to why 3D structures form so easily; Pd atoms can maintain their strong Pd–Pd bonds in a 3D structure, while reducing their electrostatic repulsion from the O-ions in the surface layer. Alternatively, the frontier orbitals on these Pd clusters may favor bonding in certain directions.

## 4.2. Diffusion of Pd clusters

Three-dimensional configurations of Pd clusters larger than the dimers, on the MgO(100) surface, are both stable energetically and also easily formed from less stable two-dimensional configurations. For example, the transitions from 2D trimer and tetramer configurations to the corresponding most stable 3D structures are shown to have barriers of only ca. 0.05 eV. This indicates that 3D structures cannot be neglected in a model of Pd cluster diffusion and growth.

We find here that Pd clusters, at least up to tetramer, are quite mobile on the MgO(100) terrace at room temperature. In a mean field diffusion model [30], monomer diffusion is assumed to be the fastest and most important for cluster growth. In order to fit this model to AFM studies of island density, the monomer diffusion barrier needs to be as low as 0.2 eV [27], so that monomer hopping is a rapid process during the initial stage of island growth above 200 K. Our calculations show that the monomer hopping barrier is somewhat higher, 0.34 eV, but that larger clusters are also mobile. The dimer can diffuse with a barrier of 0.43 eV through a partial dissociation mechanism (see Fig. 3) and the trimer can diffuse with an overall barrier of only 0.50 eV through either a flipping or walking mechanism (see Fig. 7). The tetramer diffuses with a barrier of only 0.41 eV—even lower than the trimer diffusion barrier. This decrease of the diffusion barrier from trimer to tetramer adsorbate was also predicted for Al cluster self-diffusion on Al(111) through first principle calculations, and is expected to hold for other metal/metal(111) systems [58]. Studies of Au on $Al_2O_3$ also indicate that a higher mobility of small clusters than adatoms must be considered to match experiment [59,60]. In this work, it is found that

each cluster size, from the monomer to the tetramer, have similar diffusion barriers in the range 0.34–0.50 eV. This means that entropic effects could be important to distinguish the important pathways in a kinetic analysis of growth and sintering, even at moderate temperatures.

In order to better understand and evaluate the entropic effects on the kinetics of Pd cluster diffusion, we calculated harmonic Arrhenius prefactors ($v$) for the low energy diffusion processes of each small Pd cluster. Prefactors were evaluated as the product of the stable harmonic mode frequencies of the system at the saddle point divided by those at the minimum (see Eq. 2). Frequencies were obtained using finite difference displacements of all relaxed atoms in the system, including the top MgO surface layer. The importance of surface modes on the reaction prefactors was tested by finding prefactors using a reduced Hessian matrix constructed from finite difference displacements of only the Pd atom(s). The adatom diffusion prefactor was found to be different by a factor of 2, and the tetramer by a factor of 8, indicating that it is important to include motions in the top MgO layer as we have done here. The prefactors and barriers are used to calculate rates with the harmonic form of transition state theory, Eq. (2), which are presented in Table 2. Surprisingly, the prefactors of different processes vary by more than a factor of 2000. This is quite different than recent molecular dynamics simulations using an analytic potential, which found that the prefactors for these processes "all fall in the range of $2 \times 10^{12} \text{ s}^{-1}$" [39].

Due to a high prefactor, the trimer flipping mechanism (T1-3) has a higher rate than the walking mechanism (T1-2) for all relevant temperatures (above 50 K), despite the fact that the walking mechanism has a slightly lower barrier. It is remarkable that the tetramer has a lower overall diffusion barrier than the trimer. This low barrier, combined with a high prefactor, means that the tetramer diffuses faster than the other clusters above 180 K. The high mobility of clusters as large as tetramers would give an unusual picture of mobile Pd island on the MgO(1 0 0) surface. In fact, at room temperature, our hTST rate constants suggest the tetramers should diffuse even faster than monomers.

To determine why these prefactors vary by more than 2000-fold, we analyzed the vibrational modes associated with the minimum and saddle geometries for the processes listed in Table 2. We found many soft vibrational modes in both the minima and saddle geometries, associated with collective motions of the adsorbed Pd atoms.

For the trimer walking mechanism (T1-2), the initial state has a very low mode of 11 cm$^{-1}$ associated with the frustrated rotation of the Pd cluster on the MgO surface. This mode (and other modes) is stiffer at the transition state (40 cm$^{-1}$), resulting in a low prefactor of $5 \times 10^{10} \text{ s}^{-1}$. (A typical prefactor for diffusion in solid systems is $5 \times 10^{13} \text{ s}^{-1}$). In the trimer flipping process (T1-3) the modes are comparable in the saddle geometry and the prefactor is fairly typical, $1 \times 10^{13} \text{ s}^{-1}$.

The Pd tetramer cluster has one more Pd–O bond than the trimer, and the collective rotational modes are stiffer. In the saddle geometry for the tetramer rollover process, one Pd atom loses its bond to the surface and two low rotational modes appear with frequencies of 20 cm$^{-1}$. These low modes at the saddle, which are not present in the initial minimum, lead to the very high $1 \times 10^{14} \text{ s}^{-1}$ prefactor for tetramer diffusion.

### 4.3. Kinetics of island formation

According to the energetics in Tables 1 and 2, once the oxygen vacancies saturate with monomers, mobile Pd monomers accumulate during deposition at 300 K and above. At high enough concentrations, mobile monomers will form small clusters of dimers, trimers and tetramers, instead of getting irreversibly trapped on the monomers at defects (F-centers).

Given the high mobility of the small clusters at room temperature in Table 2, one must ask whether it is the diffusion of small clusters instead of monomer hopping that dominates mass transport during Pd particle growth, by moving around and combining with monomers or clusters already trapped in F-centers (illustrated in Fig. 12). This would give a very different picture of island growth for Pd/MgO system than usually assumed.

When Pd adatoms are first deposited on the MgO(1 0 0) surface, they will hop over the surface and get trapped irreversibly as monomers in oxygen vacancies. After the vacancies become saturated, additional monomers will bind to the monomers at vacancies. The dimer binding energy on an F-center (0.56 eV) is not strong enough to hold the dimer together at 300 K and above, so that the dimers will rapidly dissociate and reform as monomers, diffusing from defect to defect. The binding to another monomer on a ter-

Table 2
The lowest diffusion barriers $\Delta E$ for Pd$_n$ ($n = 1$–4) clusters on MgO(1 0 0), the corresponding Arrhenius prefactors, $v$, and harmonic transition state theory rate $k(T)$ at two temperatures, $T$, of 200 K and 300 K

| Pd cluster (process) | $\Delta E$ (eV) | $v$ (s$^{-1}$) | $k$ (200 K) (s$^{-1}$) | $k$ (300 K) (s$^{-1}$) |
|---|---|---|---|---|
| Monomer | 0.34 | $7.4 \times 10^{11}$ | 2000 | $2 \times 10^6$ |
| Dimer (D1-2) | 0.43 | $2.5 \times 10^{11}$ | 4 | $2 \times 10^4$ |
| Trimer (T1-2) | 0.48 | $5.4 \times 10^{10}$ | 0.04 | $5 \times 10^2$ |
| Trimer (T1-3) | 0.50 | $1.1 \times 10^{13}$ | 3 | $4 \times 10^4$ |
| Tetrahedron | 0.41 | $1.3 \times 10^{14}$ | 3000 | $1 \times 10^7$ |

Traditional model in which
only monomers are mobile

Ab initio based model
with mobile small clusters

**(A)**
T < 600 K
Low
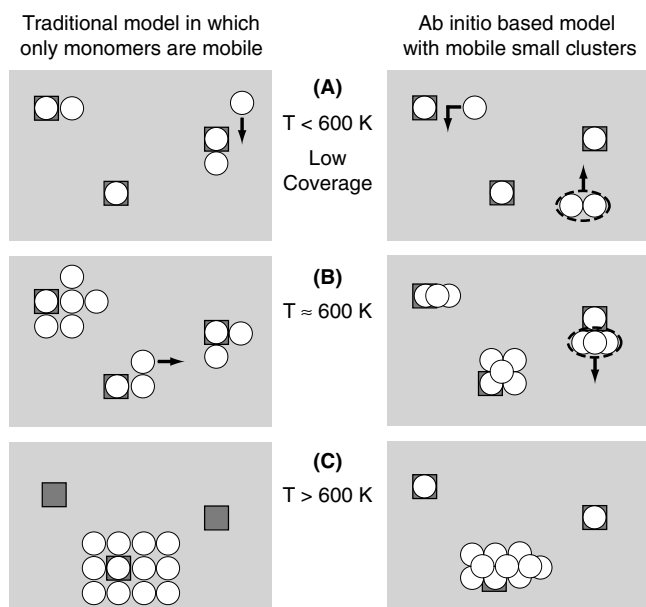Coverage

**(B)**
T ≈ 600 K

**(C)**
T > 600 K

Fig. 12. Cartoon of the expected growth in the traditional model as compared to a model based upon the present DFT energy landscape. Arrows indicate typical events that are active in the different models. (A) At low coverage and at temperatures between 200 and 600 K, monomers diffuse rapidly on the surface. In the traditional model, monomers bind to other atoms or defects irreversibly at this temperature. The DFT based model has a weak dimer binding energy so that monomer will saturate the defect sites before larger clusters form in high concentration. Monomers and dimers which form on the terrace or at defect sites continue to be mobile and diffuse or dissociate until larger clusters form. (B) At ca. 600 K ripening occurs. In the traditional model, ripening is associated with activation of dimer dissociation. In the DFT-based model, monomers and dimers are free to move or dissociate and thus quickly form larger clusters at defects. At ca. 600 K, trimers and tetramers have enough energy to dissociate from monomer-bound defects, thus rapidly forming even larger and more stable clusters at defects. (C) Above 600 K the traditional model predicts that monomers can leave defects Pd-free, and that large 2D clusters form, until at elevated temperatures, the more stable 3D clusters can finally form. DFT, however, predicts that monomers will not leave defects at temperatures below 1000 K. Small clusters, however, leave monomers behind at defects, and diffuse rapidly to coalesce into large 3D clusters at defects.

race site is also weak (0.54 eV), so these dimers on terraces will also dissociate rapidly. Thus, an equilibrium will quickly establish between mobile species on the terrace and at defects.

Over time, the islands at F-centers will grow larger. Above 600 K, trimers and tetrameters are able to break away from F-centers, leaving behind tightly bound monomers. At these high temperatures, ripening will occur rapidly. In this picture, the final configurations will still have Pd clusters trapped on those F-centers, and will show an island density that can be dominated by the defect density. This helps rationalize the experimental study of the kinetics of Pd cluster growth on MgO(100) with defects [30], where the measured island density versus flux and temperature was fitted to a model involving a single moving species, that was assumed to be monomer. The binding energy of that moving species above 600 K was found to be 1.2 eV [30].

This is clearly too large compared to the 0.56 eV calculated here for a dimer at a vacancy dissociating into a monomer at the vacancy and a diffusing monomer on a terrace, which was originally assumed to be the process associated with this 1.2 eV difference. Instead, this 1.2 eV binding energy compares much more favorably to the binding energy of bigger clusters binding energy on neutral oxygen vacancy sites which is found here by DFT to be ca. 1.0 eV (see Table 1).

Further study needs to be carried on to show how well the energetics and preexponential factors found here agree with the experimental observations. This will require kinetics simulations, which are ongoing in this lab.

The higher mobility of clusters larger than dimers, and the low adsorption energies of all clusters (less than 2.3 eV/atom) relative to the bulk cohesive energy of solid Pd (3.9 eV/atom) suggest a Volmer-Weber (or 3D) growth mode for Pd atoms on a perfect MgO(100) surface. This can be ascribed to the stronger Pd–Pd interactions as compared with Pd–MgO interactions. A 3D growth mode is consistent with experiments at temperatures between 400 and 600 K [61,62,25].

This prediction of 3D growth at room temperature should be taken with caution since there may be more complicated defects on real MgO(100) surfaces. Strong trapping effect from those defective sites may reduce the small clusters' mobility, as suggested by the studies of Pd atoms bonded on defective MgO(100) [56,43,36,51]. Therefore, island growth on real MgO(100) surfaces with defects could be very complicated and 2D islands at low coverage and low temperatures cannot be completely ruled out. Further study is needed, of the type presented in the molecular dynamics simulation of Pd island growth on MgO(100) [63], but a long time scale simulation seems to be more appropriate to disclose the predicted formation of large islands and even the growth of overlayers [64].

## 5. Conclusion

Formation and diffusion of small Pd clusters up to tetramers on MgO(100) has been studied using DFT combined with the NEB and dimer saddle point finding methods. The oxygen sites are confirmed to be the lowest energy adsorption sites for Pd adatoms and larger Pd clusters have a strong tendency to associate their first-layer Pd atoms closely with these sites but also to coalesce into 3D structures. The diffusion of Pd clusters involves stretching transitions for small clusters and 2D–3D or rollover type transitions for larger clusters. The diffusion barriers coupled with harmonic prefactors suggest a high mobility for large clusters, reflected by the faster diffusion for tetramers than trimers, dimers or monomers at room temperature. These results challenge the traditional view of monomer-dominated island growth. Vibrational mode analysis rationalizes the large variation in harmonic Arrhenius prefactors, which arise due to the stronger Pd–Pd bonding than Pd–O bonding and low energy modes of cluster rotation with respect

Table A.1
Sensitivity of the Pd monomer binding energy to calculation parameters

| Pd adsorption energy (eV) | System/parameter change |
|---|---|
| 1.375 | Reference system |
| 1.356 | $2 \times 2 \times 1$ Monkhorst-Pack $k$-point mesh |
| 1.376 | 396 eV plane wave cutoff |
| 1.380 | 36 atoms per layer in the substrate |
| 1.380 | 4 MgO layers with two relaxed |
| 1.375 | 20.5 Å vacuum gap between images |
| 1.380 | Spin polarization |
| 1.370 | Dipole correction |

Each parameter was tested by setting it more accurate than in a sufficiently converged reference system. The converged reference system for monomer adsorption has a unit cell with 24 substrate atoms per layer, 3 layers with a relaxed top layer, a 12.5 Å vacuum gap between periodic images of the MgO slab, a soft oxygen pseudo-potential with an appropriate 270 eV plane wave cutoff, $\Gamma$ point sampling of the Brillouin zone, and no spin-polarization (except for tetramer calculations) or dipole correction.

to the surface. The calculations support a Volmer-Weber or 3D island growth mode for Pd on the perfect MgO(100) surface, given the greater stability of 3D than 2D clusters, even for the trimer and tetramer. The stability of 3D clusters can be rationalized by charge density analysis of the adsorbed Pd clusters.

### Acknowledgements

### Appendix A. Convergence

The binding of a Pd atom on the MgO surface has been calculated using a range of computational parameters. Table A.1 shows the sensitivity of our calculations to increasing the accuracy of the calculation. The typical errors, on the order of 10 meV, indicate that the calculation is converged with respect to each parameter.

### References

[1] J.A. Venables, Introduction to Surface and Thin Film Processes, Cambridge University Press, Cambridge, 2000.
[2] H.J. Freund, M. Bäumer, H. Kuhlenbeck, Adv. Catal. 45 (2000) 333.
[3] C.R. Henry, Surf. Sci. Rep. 31 (1998) 235.
[4] C.T. Campbell, Surf. Sci. Rep. 27 (1997) 1.
[5] M. Valden, X. Lai, D.W. Goodman, Science 281 (1998) 1647.
[6] M. Moseler, H. Hakkinen, U. Landman, Phys. Rev. Lett. 89 (2002) 176103.
[7] T.H. Lee, R.M. Dickson, Proc. Natl. Acad. Sci. USA 100 (2003) 3043.
[8] C. Ratsch, J.A. Venables, J. Vac. Sci. Technol. 21 (2003) S96.
[9] C.T. Campbell, S.C. Parker, D.E. Starr, Science 298 (2002) 811.
[10] G.B. Mcvicker, R.L. Garten, R. Baker, J. Catal. 54 (1978) 129.
[11] E. Ruckenstein, D.B. Dadyburjor, Rev. Chem. Eng. 1 (1983) 251.
[12] P. Wynblatt, N.A. Gjostein, Progress in Solid State Chemistry, vol. 9, Elsevier Science, Amsterdam, 1975, p. 21.
[13] P. Wynblatt, N.A. Gjostein, Acta Metall. 24 (1976) 1165.
[14] C.H. Bartholomew, Stud. Surf. Sci. Catal. 111 (1997) 585.
[15] M.J.J. Jak, C. Konstapela, A. van Kreuningena, J. Chrosta, J. Verhoevena, J.W.M. Frenken, Surf. Sci. 474 (2001) 28.
[16] X. Lai, D.W. Goodman, J. Mol. Catal. A 162 (2000) 33.
[17] G. Henkelman, B.P. Uberuaga, H. Jónsson, J. Chem. Phys. 113 (2000) 9901.
[18] G. Henkelman, H. Jónsson, J. Chem. Phys. 113 (2000) 9978.
[19] G. Henkelman, H. Jónsson, J. Chem. Phys. 111 (1999) 7010.
[20] R.A. Olsen, G.J. Kroes, G. Henkelman, A. Arnaldsson, H. Jónsson, J. Chem. Phys. 121 (2004) 9776.
[21] C. Wert, C. Zener, Phys. Rev. 76 (1949) 1169.
[22] G.H. Vineyard, J. Phys. Chem. Solids 3 (1957) 121.
[23] H. Graoui, S. Giorgio, C.R. Henry, Surf. Sci. 417 (1998) 350.
[24] J.H. Harding, A.M. Stoneham, J.A. Venables, Phys. Rev. B 57 (1998) 6715.
[25] G. Renaud, A. Barbier, Surf. Sci. 435 (1999) 142.
[26] G. Renaud, A. Barbier, O. Robach, Phys. Rev. B 60 (1999) 5872.
[27] J.A. Venables, J.H. Harding, J. Cryst. Growth 211 (2000) 27.
[28] B. Hammer, Phys. Rev. Lett. 89 (2002) 016102.
[29] G. Renaud, R. Lazzari, C. Revenant, A. Barbier, M. Noblet, O. Ulrich, F. Leroy, J. Jupille, Y. Borenstein, C.R. Henry, J.P. Deville, F. Scheurer, J. Mane-Mane, O. Fruchart, Science 300 (2003) 1416.
[30] G. Haas, A. Menck, H. Brune, J.V. Barth, J.A. Venables, K. Kern, Phys. Rev. B 61 (2000) 11105.
[31] C. Barth, C.R. Henry, Phys. Rev. Lett. 91 (2003) 196102.
[32] M.-C. Wu, C.M. Trong, D.W. Goodman, Phys. Rev. B 46 (1992) 12688.
[33] P.V. Susko, A.L. Shluger, C.R.A. Catlow, Surf. Sci. 450 (2000) 153.
[34] K. Judai, S. Abbet, A.S. Wörz, A.M. Ferrari, U. Heiz, L. Giordano, G. Pacchioni, J. Phys. Chem. B 107 (2003) 9377.
[35] L. Giordano, A.D. Vitto, G. Pacchioni, A.M. Ferrari, Surf. Sci. 540 (2003) 63.
[36] L. Giordano, C.D. Valentin, J. Goniakowski, G. Pacchioni, Phys. Rev. Lett. 92 (2004) 096105.
[37] A. Bogicevic, D.R. Jennison, Surf. Sci. Lett. 515 (2002) L481.
[38] L. Xu, G. Henkelman, C.T. Campbell, H. Jónsson, Phys. Rev. Lett. 95 (2005) 146103.
[39] G. Barcaro, A. Fortunelli, F. Nita, R. Ferrando, Phys. Rev. Lett. 95 (2005) 246103.
[40] J.P. Perdew, Electronic Structure of Solids, Akademie Verlag, Berlin, 1991.
[41] D. Vanderbilt, Phys. Rev. B 41 (1990) 7892.
[42] J. Goniakowski, Phys. Rev. B 58 (1998) 1189.
[43] L. Giordano, J. Goniakowski, G. Pacchioni, Phys. Rev. B 64 (2001) 075417.
[44] A.V. Matveev, K.M. Neyman, G. Pacchioni, N. Rösch, Chem. Phys. Lett. 299 (1999) 603.
[45] I.V. Yudanov, V.A. Nasluzov, K.M. Neyman, N. Rösch, Int. J. Quant. Chem. 65 (1997) 975.
[46] V.A. Nasluzov, V.V. Rivanenkov, A.B. Gordienko, K.M. Neyman, U. Birkenheuer, N. Rösch, J. Chem. Phys. 115 (2001) 8157.
[47] R.F.W. Bader, Atoms in Molecules: A Quantum Theory, Oxford University Press, New York, 1990.
[48] G. Henkelman, A. Arnaldsson, H. Jónsson, Comput. Mater. Sci., in press.
[49] J.R.B. Gomes, F. Illas, B. Silvi, Chem. Phys. Lett. 388 (2004) 132.
[50] K.M. Neyman, S. Vent, N. Rösch, G. Pacchioni, Topics Catal. 9 (1999) 153.
[51] L. Giordano, G. Pacchioni, Surf. Sci. 575 (2005) 197.

[52] V.A. Nasluzov, V.V. Rivanenkov, A.M. Shor, K.M. Neyman, N. Rösch, Chem. Phys. Lett. 374 (2003) 487.

[53] I.V. Yudanov, S. Vent, K.M. Neyman, G. Pacchioni, N. Rösch, Chem. Phys. Lett. 275 (1997) 245.

[54] K.M. Neyman, N. Rösch, G. Pacchioni, Appl. Catal. A 191 (2000) 3.

[55] J. Goniakowski, Phys. Rev. B 57 (1998) 1935.

[56] A.V. Matveev, K.M. Neyman, I.V. Yudanov, N. Rösch, Surf. Sci. 426 (1999) 123.

[57] C. Goyhenex, C.R. Henry, J. Electron. Spectrosc. Relat. Phenom. 61 (1992) 65.

[58] C.M. Chang, C.M. Wei, S.P. Chen, Phys. Rev. Lett. 85 (2000) 1044.

[59] J. Carrey, J.-L. Maurice, F. Petroff, A. Vaurès, Phys. Rev. Lett. 86 (2001) 4600.

[60] J. Carrey, J.-L. Maurice, F. Petroff, A. Vaurès, Surf. Sci. 504 (2002) 75.

[61] C.R. Henry, M. Meunier, S. Morel, J. Cryst. Growth 129 (1993) 416.

[62] G. Renaud, Surf. Sci. Rep. 32 (1998) 5.

[63] J. Oviedo, J.F. Sanz, N. López, F. Illas, J. Phys. Chem. B 104 (2000) 4342.

[64] G. Henkelman, H. Jónsson, J. Chem. Phys. 115 (2001) 9657.